Conf-8609117--1

LA-UR -86-3182

Los Alamos National Laboratory is operated by the University of California for the United States Department of Energy under contract W-7405-ENG-36

LA-UR--86-3182

DE87 000147

TITLE NEW FISSION VALLEY FOR ^{258}Fm AND NUCLEI BEYOND

AUTHOR(S) P. Möller, J. R. Nix and W. J. Swiatecki

SUBMITTED TO for presentation at the International School-Seminar on Heavy Ion Physics, Dubna, USSR, September 23-30, 1986

DISCLAIMER

Los Alamos Los Alamos National Laboratory
Los Alamos, New Mexico 87545

NEW FISSION VALLEY FOR ^{258}Fm AND NUCLEI BEYOND

P. Möller and J. R. Nix
Theoretical Division, Los Alamos National Laboratory, Los Alamos, NM 87545

W. J. Swiatecki
Nuclear Science Division, Lawrence Berkeley Laboratory, Berkeley, CA 94720

Abstract

Experimental results on the fission properties of nuclei close to ^{264}Fm show sudden and large changes with a change of only one or two neutrons or protons. The nucleus ^{258}Fm, for instance, undergoes symmetric fission with a half-life of about 0.4 ms and a kinetic energy peaked at about 235 MeV whereas ^{256}Fm undergoes asymmetric fission with a half-life of about 3 h and a kinetic energy peaked at about 200 MeV. Qualitatively, these sudden changes have been postulated to be due to the emergence of fragment shells in symmetric fission products close to ^{132}Sn. Here we present a quantitative calculation that shows where high-kinetic-energy symmetric fission occurs and why it is associated with a sudden and large decrease in fission half-lives. We base our study on calculations of potential-energy surfaces in the macroscopic-microscopic model and a semi-empirical model for the nuclear inertia. We discuss the implications of the new fission valley on the stability of the heaviest elements.

1. Introduction

The advent of the macroscopic-microscopic Strutinsky shell-correction method[1,2] about 20 years ago made possible detailed theoretical studies of the fission process. With this method the potential energy of a nucleus can be calculated for arbitrary shapes, within given shape parameterizations. Coupled with a wealth of new experimental results this has led to an enormous increase in our understanding of nuclear shape changes during fission and also to a better understanding of the stability of elements at the end of the periodic system. For an extensive review of some of these developments see [3]. Here we apply our model to the ^{264}Fm region, for which new and somewhat unexpected experimental data are available. The first observation of the onset of symmetric fission in the region at the end of the periodic system was the study of ^{257}Fm fission by [4]. Subsequently, more observations of symmetric fission have been made in this region [5,6]. Later, more extensive measurements on ^{258}Fm and other neighboring elements by [7] have shown that there often are two components in the kinetic-energy distribution. Our goal is to understand the nature of the fission process for the nuclei for which these new data are available and then to make predictions of properties of other nuclei in the vicinity of ^{264}Fm and of fission half-lives for heavier even nuclei. We take information about the experimental fission half-lives from [8,9,10,11,12].

2. Macroscopic-microscopic model

Our model is of the macroscopic-microscopic type and has been discussed extensively in [13,14,15,16]. In the macroscopic-microscopic model the nuclear energy, which is calculated as a

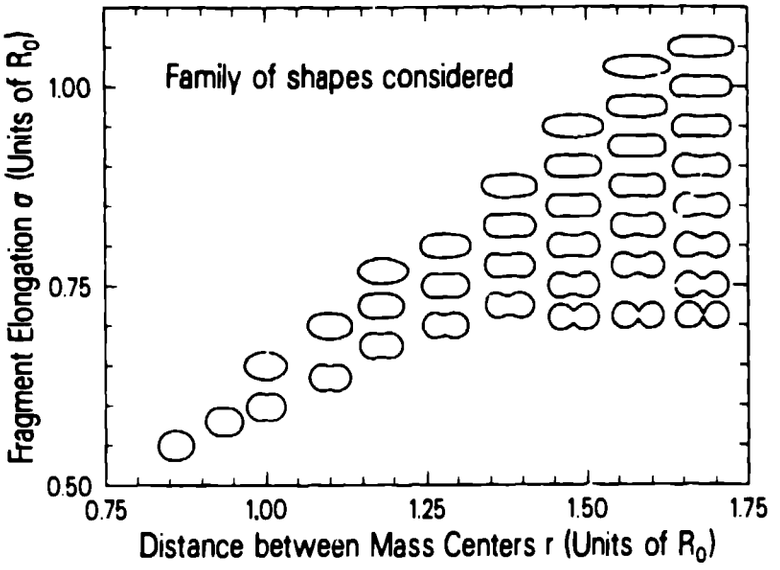

Figure 1: Nuclear shapes corresponding to potential-energy surfaces. The lower boundary corresponds to two overlapping spheres for $r \leq 1.59$ and to scission configurations for $r \geq 1.59$.

function of shape, proton number Z and neutron number N, is the sum of a macroscopic term and a microscopic term. Thus the total nuclear potential energy can be written as

$$E(Z, N, \text{shape}) = E_{\text{macr}}(Z, N, \text{shape}) + E_{\text{micr}}(Z, N, \text{shape}) \quad (1)$$

We use a Yukawa-plus-exponential model for the macroscopic term and a folded-Yukawa single-particle potential as a starting point for calculating the microscopic term. We use the model with the parameter set that was determined in the investigation [14], which calculated ground-state masses for 4023 nuclei and fission barriers for 28 nuclei throughout the periodic system. The root-mean-square deviation between experimental and calculated ground-state masses was 0.835 MeV for a set of 1323 masses and 1.331 MeV for the 28 fission barriers. Many other properties such as ground-state deformations are also well described by the model, as is extensively discussed in [16]. The model represents a unified approach to the study of many features of nuclear structure, fission and heavy-ion reactions.

Two shape parameterizations are at present implemented in the model. One is the three-quadratic-surface parameterization [17] and the other is the ϵ parameterization [18]. The latter is the more suitable one for investigating ground-state shapes. In the fission half-life calculations below we always take the ground-state energy from calculations using the ϵ parameterization. In the calculation of potential-energy surfaces it is of considerable importance to select shapes that are related to the processes that are studied. We use the three-quadratic-surface parameterization in the calculation of potential-energy surfaces that we perform to search for the two fission valleys. This parameterization is the most suitable one for generating shapes beyond ground-state shapes that are of interest in fission, in particular for generating shapes close to scission configurations. However, we have also performed calculations of potential-energy surfaces as functions of ϵ_2, ϵ_4 and mass-asymmetric ϵ_3 shape coordinates. It turns out that along the old path the lowest saddle-point energies are obtained in that parameterization partly for the reason that more shape degrees of freedom are investigated. Therefore, we use those results below in the calculation of fission half-lives along the old path.

It is not very useful to display calculated results as functions of quantities that are related to the geometry of the shape, such as the ratio of the major to minor axis of the end bodies or the distances between the centers of the quadratic surfaces that generate the shape of the ends of the

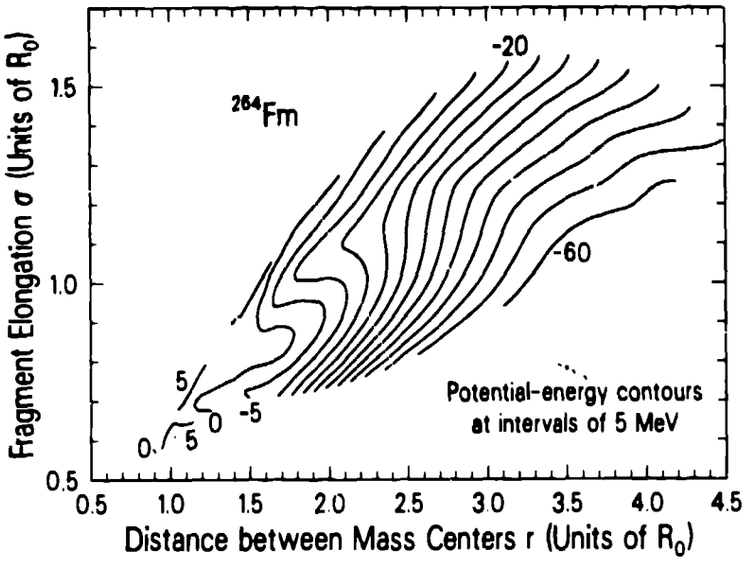

Figure 2: Valleys leading to compact and normal scission shapes for ^{264}Fm.

nucleus, because the relation between these quantities and the actual shapes is very non-linear. We therefore display the calculated results as functions of moments of the shape. This has the additional advantage that results from calculations using different shape parameterizations can be displayed as functions of the same quantities. The two most important symmetric moments of the matter distribution are defined by

$$r = 2\int_{z\geq 0} z\rho(\mathbf{r})d^3r \Big/ \int_{z\geq 0} \rho(\mathbf{r})d^3r$$

and

$$\sigma = 2\left[\int_{z\geq 0}(z-\frac{1}{2}r)^2\rho(\mathbf{r})d^3r \Big/ \int_{z\geq 0} \rho(\mathbf{r})d^3r\right]^{\frac{1}{2}} \qquad (2)$$

Below we display calculated total potential energies as functions of r and σ. Both in the figures and in the paper we use units in which the equivalent sharp radius R_0 of the spherical nucleus is 1.

The three-quadratic-surface parameterization allows the variation of three symmetric and two asymmetric shape coordinates. We here limit our study to symmetric shapes. This leaves us with the three symmetric shape coordinates σ_1, σ_2 and σ_3 [17]. They are related to the overall separation, neck size and eccentricity, respectively, of the end bodies. One realizes that only a small deviation from sphericity of the end fragments removes the influence on the shell effect for magic or near magic numbers. To study the full effect of the magic fragment shell effects we therefore fix σ_3 at 1, which corresponds to spherical ends and vary only σ_1 and σ_2.

We study all shapes that are accessible within the parameterization with $\sigma_3 = 1$. Our results are displayed as functions of the two moments r and σ given by eq. (2). We show some examples of the actual shapes considered in fig. 1. Most previous theoretical studies of fragment shell effects suffer from the two deficiencies that (1) the parameterization is incapable of generating the two-touching sphere configuration and of exercising independent control of the shapes of the ends of the nucleus and (2) the liquid-drop model for the surface energy is inappropriate for studying shapes with well-developed necks.

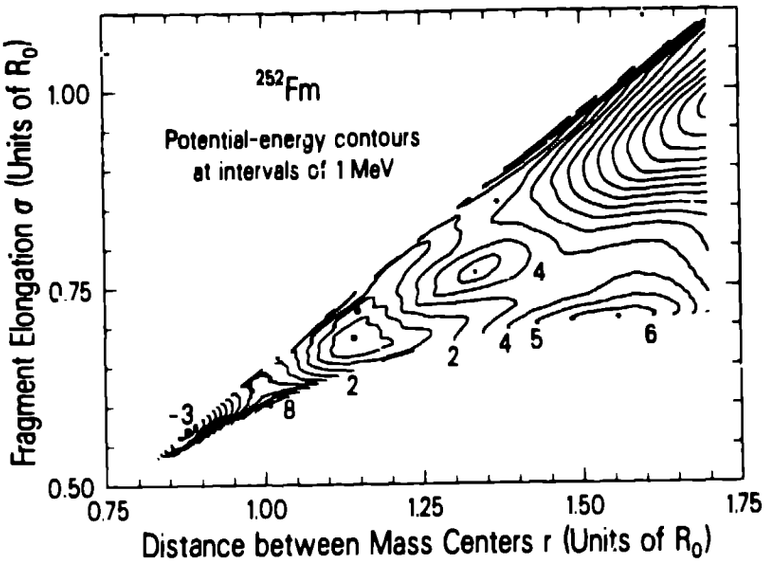

Figure 3: Mountains, saddle points, valleys and minima for ^{252}Fm. Two saddles lead to the normal fission valley in the upper right corner. The tangent-sphere configuration is blocked by a mountain.

3. Calculated results

We display the calculated energies in the form of contour diagrams. In fig. 2 we show a contour diagram for ^{264}Fm. For this nucleus there is no second minimum. Instead, a short but deep valley starts at the first saddle and leads directly to the two-touching-sphere configuration. This short, deep valley is separated by an 8 MeV high ridge from another valley in the upper part of the diagram. On the ridge there is a mountain at $r = 1.41$, $\sigma = 0.83$ and above this mountain there is a slightly lower saddle leading into the upper valley. The upper valley is similar to valleys found in plots of the macroscopic energy only. The lower valley has clearly been created by fragment shell effects. Using terminology from [7], the lower valley is fragment-shell-directed and the upper one is liquid-drop-like. The upper valley is the old valley and the lower valley is the new valley.

To show in greater detail both the emergence of the new valley and the transition region from fission in the old valley to fission in the new valley, we display contour maps for ^{252}Fm and ^{256,258,260}Fm in figs. 3–6. The solid dots in the figures indicate local minima and the plus signs indicate local maxima. Scanning through figs. 3–6 we see that ^{256}Fm appears to be a transition nucleus. Here the saddle point on the lower side of the mountain centered at $r = 1.34$, $\sigma = 0.77$ is the lower saddle. The plus sign in this saddle region indicates the presence of a small hill. Motion to either side of this hill seems about equally possible. Although there is a low hill at the configuration of two touching spheres, a valley just above this hill leads to compact scission just beyond the two-touching-sphere configuration. It also seems possible that the shape evolution proceeds from the lower saddle to the old valley in the upper part of the diagram. We note that the upper saddle is lowered somewhat by mass-asymmetric shape degrees of freedom [19], which provides a mechanism for the predominantly mass-asymmetric fission that is observed experimentally. The low-kinetic-energy mass-asymmetric fission into the old valley could proceed entirely along the upper valley and its mass-asymmetric saddle or initially follow the lower valley below the mountain peak and then turn back into the old valley. In the latter case the mass asymmetry would have to develop at the lower saddle or at a later stage beyond the last saddle in the older valley.

For the nucleus ^{258}Fm the bottom saddle is about 1.5 MeV lower than the upper saddle. There is a tiny hill at the configuration of two touching spheres, but fission across the saddle

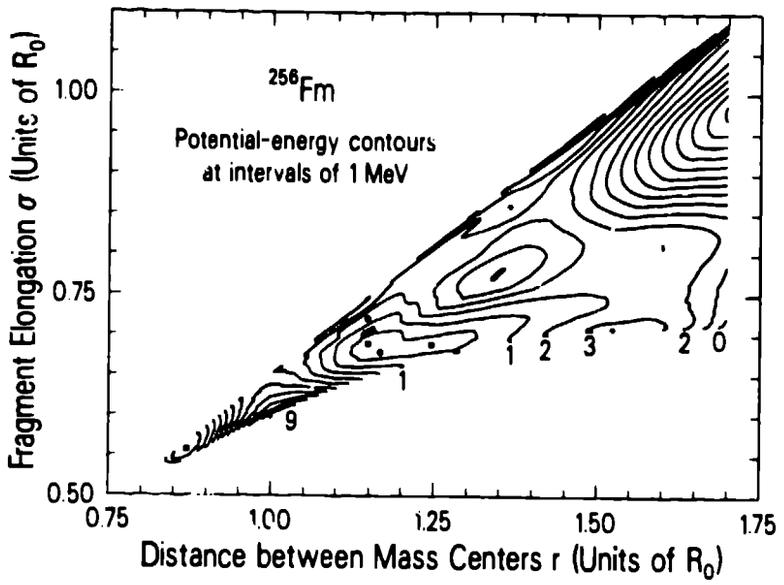

Figure 4: Transition nucleus. Initially the lower valley is probably followed. Later, in a majority of cases the nucleus switches back to the old valley, but may also in a few cases penetrate the barrier to compact shapes.

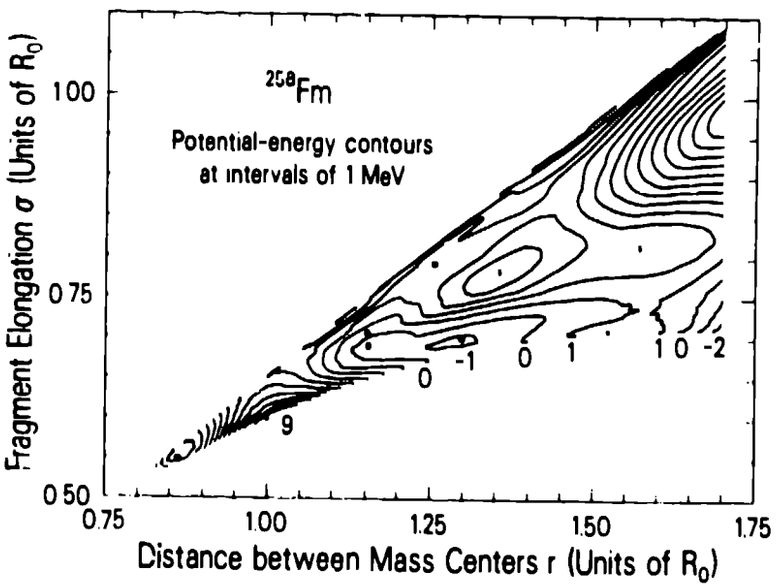

Figure 5: Ridge separating the old and new fission valleys. Most events will lead to compact scission but in some cases the low ridge may be penetrated, leading to low-kinetic-energy fission. The second minimum has now shifted outwards to $r = 1.30$, $\sigma = 0.70$, which raises the possibility of the existence of a molecular state at this new location.

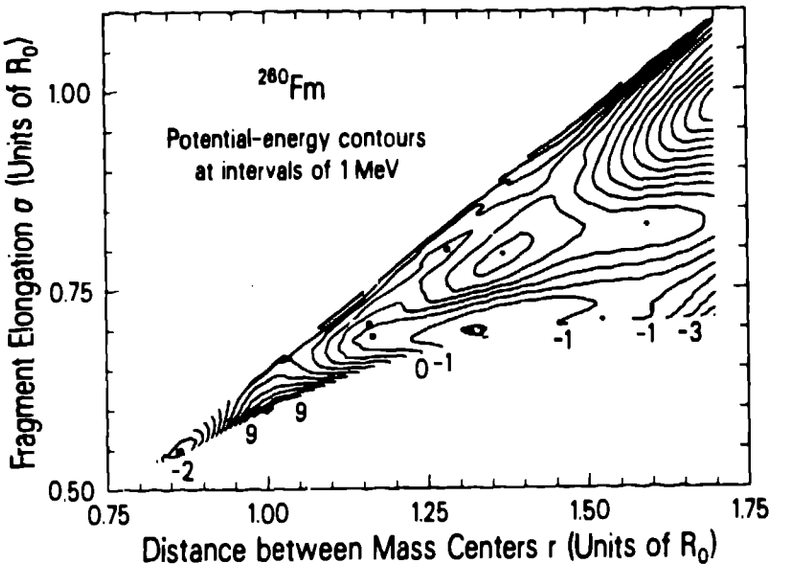

Figure 6: Higher ridge, deeper new valley and changed location of second minimum.

just above this hill leads to the new valley and scission just beyond the two-touching-sphere configuration. There is a 1.2 MeV high ridge separating this valley from the old valley above. Since the ridge is low, some trajectories may penetrate this ridge and lead to the old valley. This strucure is compatible with the observed fission characteristics of this nucleus. For ^{260}Fm the ridge separating the old and new valleys has grown to a height of 3 MeV. The considerable height of the ridge should block all access to the old valley.

It has been proposed that the rapid change in half-life when going from ^{256}Fm to ^{258}Fm is due to the disappearance of the second saddle in the barrier below the ground-state energy. Fission through only one barrier, the first, gives very good agreement with the observed short half-life of ^{258}Fm [20,21]. However, one may ask if and how the fission half-life is connected to the change in the other fission properties at this transition point, namely to the change to symmetric fission and to high kinetic energies. To calculate fission half-lives it is necessary to know the potential energy, the inertia associated with the motion through the barrier and the path from the ground state through the barrier. Because of uncertainties in and complexities of microscopic models for the inertia, we here use a semi-empirical approach. In a one-dimensional WKB spontaneous-fission model the fission half-life is connected to the penetrability by [22,23]

$$T_{sf} = 10^{-38.04}\ \mathrm{y}/P \tag{3}$$

where the value $\omega_0 = 1$ MeV/$\hbar$ is used for the frequency of assaults on the barrier. The probability P of penetrating the barrier $V(r)$ at the energy E_0 is given by [24]

$$P = \frac{1}{1+e^{K}} \tag{4}$$

where

$$K = 2\int_{r_1}^{r_2}\left\{\frac{2B_r(r)}{\hbar^2}\left[V(r)-E_0\right]\right\}^{1/2} dr \tag{5}$$

Here $V(r)$ is the barrier energy along the selected path. The penetration energy E_0 is the ground-state energy plus the zero-point energy in the fission direction at the ground state.

The function $B_r(r)$ is the inertia with respect to r associated with motion in the fission direction. An important aspect of the semi-empirical approach is to deduce asymptotic properties of the semi-empirical inertia from some general arguments about the expected properties of the

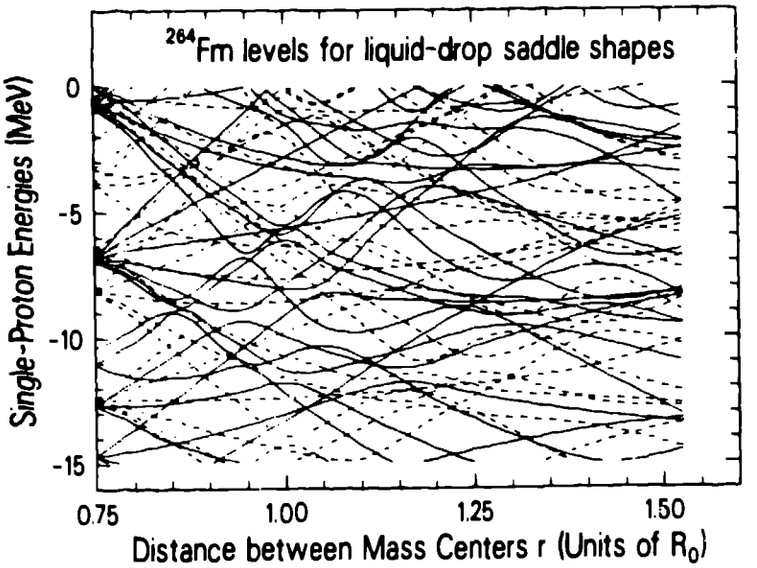

Figure 7: Single-proton levels corresponding to fission in the old valley.

inertia at small and large r values. Thus, at large distances we expect $B_r(r)$ to approach the value $\frac{1}{4}M$ appropriate to separated symmetric fragments. At small r values the inertia is expected to be considerably higher than what is given by a hydrodynamical irrotational-flow model, due to microscopic quantum-mechanical effects. In the semi-empirical model these asymptotic constraints are taken into account by relating the inertia B_r to the inertia B_r^{irr} corresponding to irrotational flow by [23]

$$B_r - \mu = k(B_r^{\mathrm{irr}} - \mu) \tag{6}$$

where k is a semi-empirical constant and μ is the reduced mass of the final symmetric fragments. We approximate numerical results for eq. (6) by [25]

$$B_r^{\mathrm{irr}} - \mu = \frac{17}{15}\mu \exp\left[-\frac{128}{51}\left(r - \frac{3}{4}\right)\right] \tag{7}$$

In our case, we use the value $k = 16$, which was determined in [25] from an adjustment to five actinide fission half-lives. In that adjustment the root-mean-square deviation between the logarithms of the calculated and experimental half-lives was 2.5.

In calculating fission half-lives along the old valley we find theoretically about the same fission half-life, 1 y, for nuclei ranging from ^{252}Fm to ^{260}Fm, in violent disagreement with the experimental data for ^{258}Fm. The discrepancy for this nucleus is 11 orders of magnitude. Our first thought as to the reason for this huge disagreement was that the calculated barrier was wrong. In the old valley we had obtained a value of 4 MeV for the height of the second barrier. One possible source of error in the second barrier height could be incorrect values of the parameters of the macroscopic model. We investigated this possibility within the framework of a macroscopic-microscopic model. Our conclusion was that the parameters had been well determined by the original adjustment to the data and that it was not possible to lower the calculated barrier by readjusting the macroscopic-model parameters.

Our second thought as to the reason for the ^{258}Fm disagreement was that the fission barrier in the proposed new valley might be lower and yield correspondingly lower half-lives, in better agreement with the experimental data. The results obtained in fig. 5 seem to partly bear this hypothesis out The barrier here is 1.5 MeV lower at the bottom saddle point than at the upper saddle point. However, the upper saddle point is lowered 1 MeV by mass-asymmetric shape degrees of freedom. When we evaluate the fission half-life along the new valley for ^{258}Fm, we

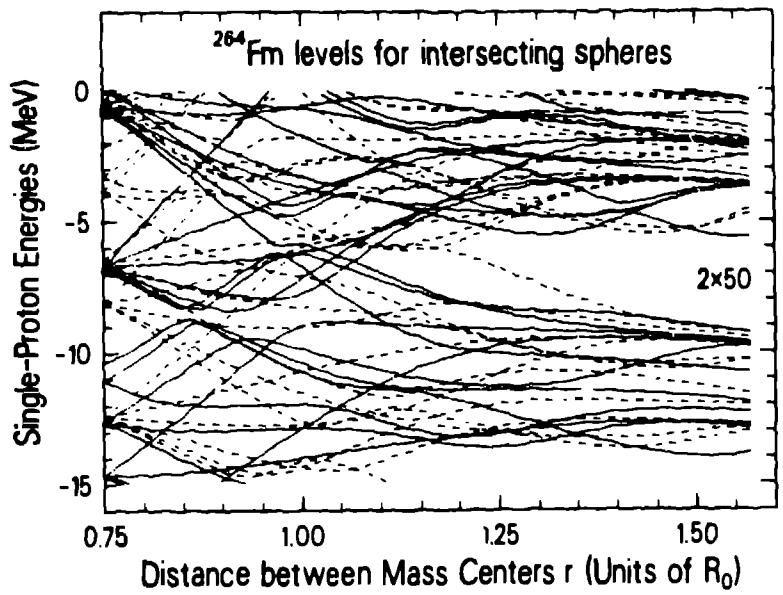

Figure 8: Single-proton levels corresponding to fission in the new valley.

obtain 10^8 y. We find that the bottom saddle point is stable with respect to mass asymmetry and to deviations from spherical end shapes.

Leander pointed out to us [26] that one would expect the inertia B_r to be radically different in the new valley compared to the old valley, because in the new valley the structure of the final system emerges very early. Earlier, Mosel *et al.* [27] gave similar arguments for a much smaller inertia in the new valley, compared to the old valley. However, no calculation of fission half-lives was carried out, nor was any inertia for the new valley calculated or proposed. In figs. 7 and 8 we show proton single-particle levels for shapes evolving from a spherical shape into the old and new valley, respectively. It is immediately clear from inspecting figs. 7 and 8 that the level structures in the two valleys are radically different. For the new valley it is clear that our current form of the semi-empirical inertia is inadequate. In its present form the inertia reaches the limiting value $\frac{1}{4}M$ at infinity. In fig. 8 we see that the magic gap $Z = 50$ extends into such compact shapes as $r = 1.20$ and to a somewhat lesser extent as far as $r = 1.07$. Over this entire region the levels are almost parallel and already here, long before separation, the inertia should be very close to its limiting value of $\frac{1}{4}M$.

To fulfill the above limiting conditions for the new valley in a simple way we propose for the inertia in the new valley

$$B_r - \mu = f(r, r_{sc})k(B_r^{lim} - \mu) \tag{8}$$

where

$$f(r, r_{sc}) = \begin{cases} \left(\frac{r_{sc} - r}{r_{sc} - 0.75}\right)^m , & r \leq r_{sc} \\ 0 , & r \geq r_{sc} \end{cases} \tag{9}$$

and r_{sc} is the r value where the new valley reaches scission, which in our investigation here is set equal to the r value for two touching spheres, which is $r_{sc} = 1.59$. The inertia in eq. (8) has the property that it approaches the limiting value horizontally for $m \geq 2$. Also at the ground state one can expect the inertia to be lower for shape changes that evolve towards the new valley, compared to shape changes that lead to the old valley. This can occur because the inertia is not related to the values of the shape coordinates themselves but instead to their derivatives, or more precisely, to the direction of change of the shape coordinates. Quantitative support for this can

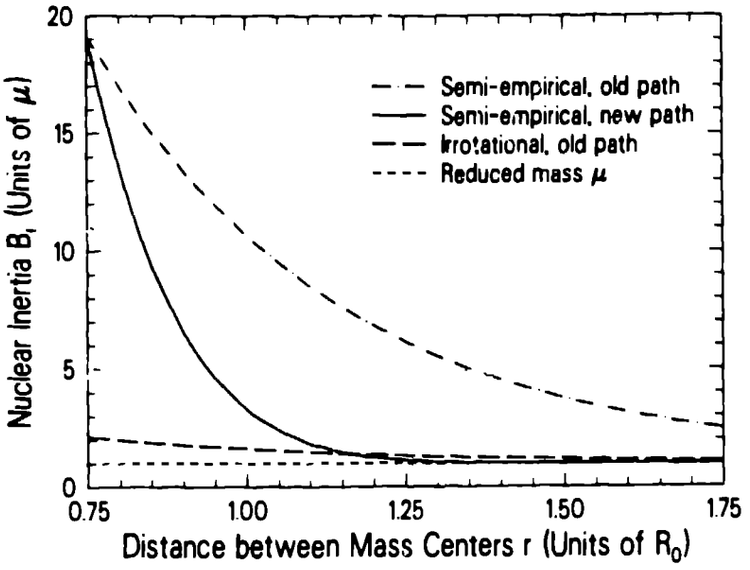

Figure 9: Comparison between the semi-empirical inertia along the old path, the semi-empirical inertia along the new path, the irrotational inertia along the old path and the reduced mass μ.

be found in the level diagrams in figs. 7 and 8. Often the distance between levels at level crossings is larger in fig. 8 than in fig. 7.

We have calculated the fission half-life for ^{258}Fm along the new valley with the inertia given by eqs. (8) and (9). A high exponent m will make the inertia in the new valley approach the limiting value early and also decrease the half-life for fission in the new valley. With the choice $m = 4$ we obtain a half-life of 10^{-7} y for ^{258}Fm in the new valley. Although this is 4 orders of magnitude larger than the experimental result it is nevertheless fairly close to the experimentally observed value of 10^{-11} y and for the next even Fm isotope ^{260}Fm we obtain a half-life of 42 ms. The semi-empirical inertias for the old and new valleys are plotted in fig. 9.

The proposed inertia for the new valley is most appropriate for Z near 100 and N near 164. Below we see that the new valley remains for Z and N values rather far from these values. For such nuclei we expect that the inertia is higher than the one proposed here. However, in the absence of a microscopic model for the inertia in the new valley we consistently use the simple prescription given by eqs. (8) and (9). This leads to some underestimate of the fission half-lives far from ^{264}Fm.

In figs. 10 and 11 we present contour diagrams similar to those for Fm shown in figs. 3–6 but for ^{258}No and ^{272}108, respectively. According to our discussion above, if high kinetic energies are a signature of fission along the lower path and low kinetic energies a signature of fission along the upper path, then low-kinetic-energy events should have long half-lives and high-kinetic-energy events should have short half-lives. In addition to ^{258}Fm, data in the region of interest are available for only two other even nuclei, namely ^{258}No and ^{260}Rf [7]. The first nucleus, ^{258}No, undergoes symmetric fission with a fairly narrow symmetric mass distribution and low kinetic energies but with a small high-kinetic-energy component. Our argument above led us to expect a long half-life for low kinetic energies. However, a look at fig. 10 provides an understanding of the data for ^{258}No. The barrier is penetrated along the lower path, with its low inertia, and after the saddle at about $r = 1.35$, $\sigma = 0.72$ and the shallow minimum beyond, at $r = 1.48$, $\sigma = 0.75$, the nucleus can decide to go either into the new valley or into the old valley. This perhaps unexpected phenomenon of initially following the new valley and then returning to the old valley we call *switchback*.

Since both high-kinetic-energy and low-kinetic-energy events are seen for ^{258}No, the half-lives

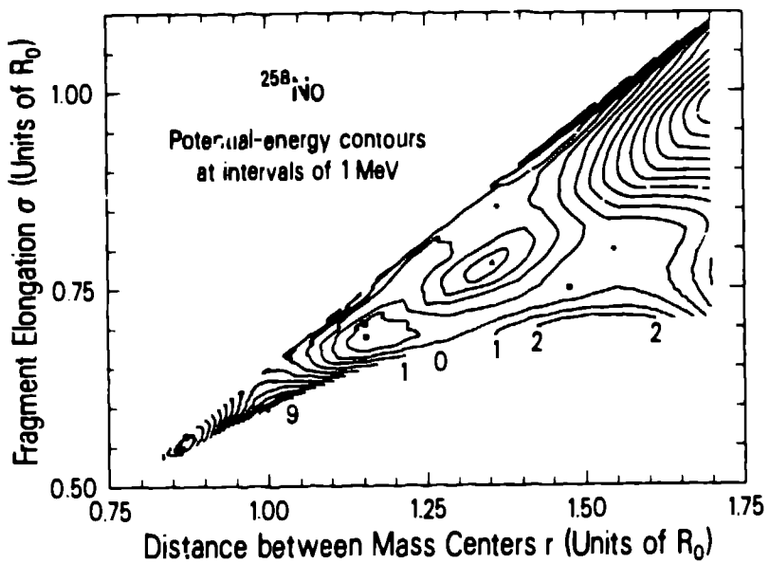

Figure 10: Transition nucleus. Experimentally mostly low-kinetic-energy fission is seen for this nucleus, but there are also appreciable high-kinetic-energy events observed.

for fission into the old valley and into the new valley are of comparable magnitude, experimentally. To study the switchback to the old valley would require a knowledge of the inertia for this part of the fission path, which we do not have. However, we do have a simple model for the inertia for fission along the new path into the new valley. With $m = 4$ we obtain a fission half-life of 420 ms. The half-life calculated along the old valley is 45 m. This can be compared to the observed half-life of 1.2 ms. Thus, along the old valley the calculated half-life is more than six orders of magnitude larger than the observed half-life. Since two components are observed experimentally in the kinetic-energy distributions in the fission of these two elements the fission half-lives corresponding to the two components cannot differ by more than one or two orders of magnitude. We conclude that this indicates that the *same* barrier is penetrated in the two cases, except for a tiny portion at the end of the penetration process.

There is an additional argument for interpreting the switchback as the mechanism for bimodal fission that is independent of the accuracy of the theoretical fission half-life model. Experimentally, the fission half-lives change extremely rapidly from nucleus to nucleus in this region. For instance, from ^{256}Fm to ^{258}Fm the half-life changes by seven orders of magnitude. At a transition point one might expect the half-lives for fission through the two different barriers to be similar, as a general rule. However, when the change across the transition point is seven orders of magnitude it is unlikely that the two half-lives are equal to within two orders of magnitude. It might perhaps occur in one case but experimentally there are four cases of observed bimodality and it is extremely unlikely that the two barriers have approximately the same half-life in all four cases with such violent changes in half-lives across the transition points.

In table 1 we present calculated fission half-lives for even nuclei from Cf to $Z = 110$. The fission half-lives have been calculated for both the old and new paths. In some cases the compact scission shapes are not accessible because a mountain at this configuration blocks access and clearly pushes the nucleus back into the old valley. These cases are indicated in the table by (s) for switchback. In these cases we have calculated the fission half-lives by integrating along a path that leads back into the old valley. The inertia we have used in these few cases is the one that is appropriate to the new valley and, as pointed out above, the calculated half-lives along the switchback are therefore *underestimated*. The contour maps and the results in table 1 show that we have a good quantitative understanding of the fission process for these heavy elements. We

TABLE 1
Comparison of fission half-lives calculated for the normal and new paths with experimental values

Z	N	A	Calc. for old path		Calc. for new path		Exp.	
98	156	254	1.0	y			60.5	d
	158	256			1.5	d	12	m
	160	258			1.2	m		
100	152	252	42	d	(s) 10	s	150	y
	154	254	1.3	y	(s) 30	s	222	d
	156	256	190	d	7.7	m	2.86	h
	158	258	2.7	y	9.3	s	0.38	ms
	160	260	13	y	42	ms		
102	152	254	11	s			24	h
	154	256	3.9	m	(s) 17	ms	23	m
	156	258	45	m	420	ms	1.2	ms
	158	260	14	d	540	ms		
	160	262	85	d	1.7	ms		
	162	264	19	y	21	μs		
104	152	256	46	μs			5	ms
	154	258	2.6	ms	(s) 960	μs	11	ms
	156	260	73	ms	(s) 520	μs	20	ms
	158	262	3.3	s	300	μs	63	ms
	160	264	2.8	d	2.0	ms		
	162	266	3.9	y	44	μs		
106	152	258	1.3	ms				
	154	260	470	μs	(s) 15	μs	7	ms
	156	262	25	s	32	μs		
	158	264	1.0	m	19	μs		
	160	266	14	h	5.1	μs		
	162	268	21	y	160	μs		
108	154	262	170	μs	7.2	μs		
	156	264	1.2	ms	4.4	μs	> 100	μs
	158	266	57	ms	28	μs		
	160	268	22	s	9.4	μs		
	162	270	3.3	y	82	μs		
	164	272	18	d	71	μs		
110	158	268	190	ms				
	160	270	28	s				
	162	272	8.5	h				
	180	290	10^{12}	y				

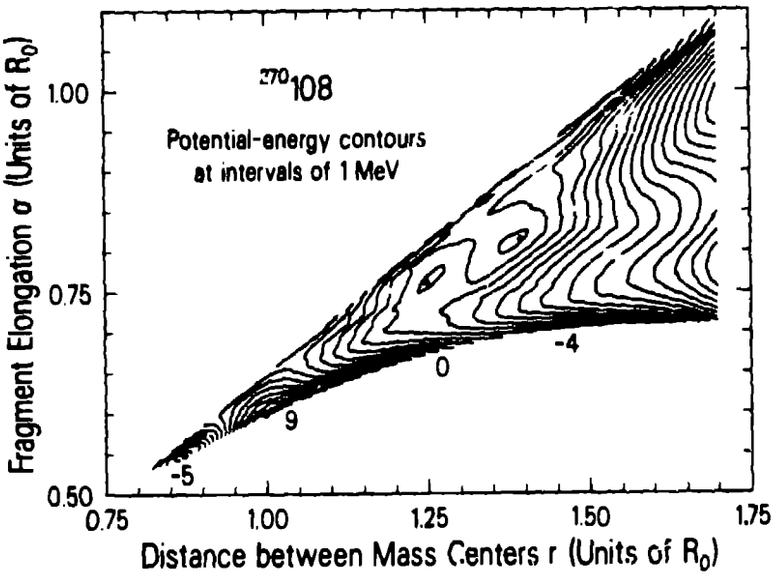

1: The new valley is present also at this Z value and may lead to fission half-lives in the
e on the "rock".

hat the half-lives marked (s) are severely underestimated and that the shorter half-life cases is always obtained by fission along the upper path. For cases not marked by (s) we culated the half-life for fission into compact shapes along the lower path. If we assume nuclei marked (s) fission always takes place along the upper valley and that in the other path with the shortest half-life is chosen, then we find that the calculations are within ree orders of magnitude from the experimental data in all cases. However, we should for nuclei without the (s) the fission path may divide and lead both into compact shapes the old valley according to our discussion above. In fig. 12 we show shapes along various ths for ^{258}Fm.

been predicted [28] that there is a rock of stability in the vicinity of ^{272}110. However, = 162 is close to $N = 2 \times 82$, where the new fission valley leads to considerably shorter lf-lives than was expected earlier, this rock may be less stable than previously thought, ecay was thought to be the dominating mode of decay on the rock. In table 1 we find that cted fission half-lives for ^{268}106 and ^{270}108 are both about 100 μs. Since we expect that we mate the inertia in the new valley this far from ^{264}Fm it is perhaps reasonable to expect half-life of about 10 or 100 *ms* for these nuclei and also for ^{272}110. We draw a similar n from comparing the predicted and experimental half-life for ^{262}Rf. Unfortunately, this at the expected fission half-lives for elements on the rock are uncomfortably close to the α half-lives. This may complicate the design of experiments to reach the rock.

4. Heavy-ion reactions

otential-energy surfaces for those nuclei where the fragment-shell effects lead to a new istrate the anticipated beneficial influence of magic target-projectile combinations on d evaporation-residue cross sections in heavy-ion reactions.

the magicity of the fragments lowers the energy of the two-touching-sphere configuration o what it would be in the absence of shell effects. It follows that in cases where a d nucleus is formed by a dynamical descent from the two-touching-sphere configuration, ound nucleus will be formed with less excitation energy than if fragment shell effects were The resulting relatively cold compound nucleus has then a better chance of surviving,

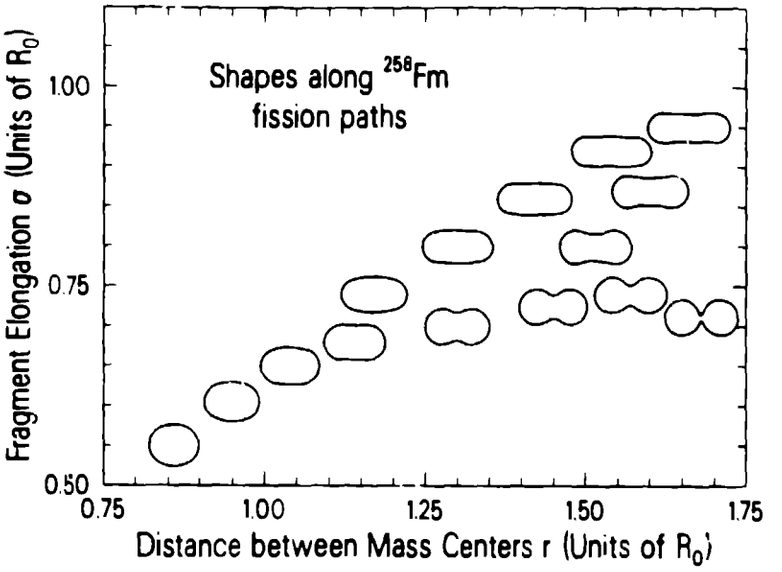

Figure 12: Shapes along old, new and switchback fission paths. The bottom shapes are along the new path and the top shapes are along the old path, which we feel is not involved in the fission of ^{258}Fm. The shapes breaking off from the bottom path are along the switchback path, which leads back into the old valley.

without fissioning, the subsequent stage of de-excitation by particle emission. The result is an enhancement of evaporation-residue cross sections.

The second, more subtle effect, has to do specifically with the appearance of a *valley* in the potential-energy surface and the effect this has on minimizing the need for an extra push to fuse heavy nuclei [29,30]. The new valley in a potential-energy surface such as in fig. 2 demonstrates that fragment shell effects such as those in ^{132}Sn can survive in configurations with even a fairly large window beween the two halves, thus providing a mechanism for mitigating the extra-push hindrance in reactions beween near magic nuclei. We believe it is quite likely that this mechanism is responsible for the anomalously low hinderance factors in fusion reactions such as ^{48}Ca + ^{208}Pb [31,32,33]

5. Summary

In summary, the most important new results that we have found are:

- For elements close to ^{264}Fm a deep valley leading to compact scission shapes is a very prominent feature in the calculated potential-energy surfaces.
- From a study of single-particle level diagrams and a calculation of fission barriers and fission half-lives we conclude that there is a much lower inertia associated with fission in the new valley than in the old valley.
- Fission may initially proceed along the new valley and *switchback* to the old valley at a later stage during the process.
- We propose that the short half-life of ^{258}Fm is due to the low inertia in the new valley and *not* to the disappearance of the second peak in the fission barrier.
- The new valley is present up to at least $Z = 108$ and lowers fission half-life predictions for elements on the rock centered around ^{272}110, relative to earlier predictions.

- Calculated fission half-lives agree to within three orders of magnitude with experimental data for elements from Cf to $Z = 108$ for which $N \geq 152$.

We would like to acknowledge many valuable discussions on the theoretical aspects of this investigation with G. A. Leander, W. D. Myers, J. Randrup and A. J. Sierk and on the experimental side with D. C. Hoffman, E. K. Hulet and P. Armbruster.

P. Möller would like to thank the Los Alamos National Laboratory, the Lawrence Livermore National Laboratory and the Lawrence Berkeley Laboratory for their hospitality during the past year and the support that made this investigation possible. This work was supported by the U. S. Department of Energy.

References

1. V. M. Strutinsky, Nucl. Phys. **A95** (1967) 420.

2. V. M. Strutinsky, Nucl. Phys. **A122** (1968) 1.

3 S. Bjørnholm and J. E. Lynn, Rev. Mod. Phys. **52** (1980) 725.

4. J. P. Balagna, G. P. Ford, D. C. Hoffman and J. D. Knight, Phys. Rev. Lett. **26** (1971) 145.

5. E. K. Hulet, R. W. Lougheed, J. H. Landrum, J F. Wild, D. C. Hoffman, J. Weber and J. B. Wilhelmy, Phys. Rev. **C21** (1980) 966.

6. D. C. Hoffman, J. B. Wilhelmy, J. Weber, W. R. Daniels, E. K. Hulet, R. W. Lougheed, J. H. Landrum, J. F. Wild and R. J. Dupzyk, Phys. Rev. **C21** (1980) 972.

7. E. K. Hulet, J. F. Wild, R. J. Dougan, R. W. Lougheed, J. H. Landrum, A. D. Dougan, M. Schädel, R. L. Hahn, P. A. Baisden, C. M. Henderson, R. J. Dupzyk, K. Sümmer and G. R. Bethune, Phys. Rev. Lett. **56** (1986) 313.

8. Table of Isotopes, 7th edition, edited by C. M. Lederer and V. S. Shirley (Wiley, New York, 1978).

9. J. K. Tuli, Nuclear Wallet Cards, National Nuclear Data Center, Brookhaven National Laboratory (1985).

10. L. P. Somerville, M. J. Nurmia, J. M. Nitschke, A. Ghiorso, E. K. Hulet and R. W. Lougheed, Phys. Rev. **C31** (1985) 1801.

11. G. Münzenberg, S. Hofmann, H. Folger, F. P. Hessberger, J. Keller, K. Popensieker, B. Quint, W. Reisdorf, K.-H. Schmidt, H. J. Schött, P. Armbruster, M. E. Leino and R. Hingmann, Z. Phys. **A322** (1985) 227.

12. G. Münzenberg, P. Armbruster, G. Berthes, H. Folger, F. P. Hessberger, S. Hofman, K. Poppensieker, W. Reisdorf, B. Quint, K.-H. Schmidt, H. J. Schött, K. Sümmerer, I. Zychor, M. E. Leino, U. Gollerthan and E. Hanelt, Z. Phys., to be published.

13. M. Bolsterli, E. O. Fiset, J. R. Nix and J. L. Norton, Phys. Rev. **C5** (1972) 1050.

14. P. Möller and J. R. Nix, Nucl. Phys. **A361** (1981) 117.

15. P. Möller and J. R. Nix, At. Data Nucl. Data Tables **26** (1981) 165.

16. R. Bengtsson, P. Möller, J. R. Nix and Jing-ye Zhang, Phys. Scr. **29** (1984) 402.

17. J. R. Nix, Nucl. Phys. **A130** (1970) 241.

18. P. Möller, S. G. Nilsson and J. R. Nix, Nucl. Phys. **A229** (1974) 292.

19. P. Möller and J. R. Nix, Nucl. Phys. **A229** (1974) 269.

20. J. Randrup, C. F. Tsang, P. Möller, S. G. Nilsson and S. E. Larsson, Nucl. Phys. **A217** (1973) 221.

21. J. Randrup, S. E. Larsson, P. Möller, S. G. Nilsson, K. Pomorski and A. Sobiczewski, Phys. Rev. **C13** (1976) 229.

22. S. G. Nilsson, C. F. Tsang, A. Sobiczewski, Z. Szymański, S. Wycech, C. Gustafson, I.-L. Lamm, P. Möller and B. Nilsson, Nucl. Phys. **A131** (1969) 1.

23. E. O. Fiset and J. R. Nix, Nucl. Phys. **A193** (1972) 647.

24. N. Fröman and P. O. Fröman, JWKB Approximation (North-Holland, Amsterdam, 1965) chap. 9, sect. 1, pp. 92-97.

25. P. Möller and J. R. Nix, Phys. Rev. Lett. **37** (1976) 1461.

26. G. A. Leander, private communication (1986).

27. U. Mosel and H. W. Schmitt, Phys. Rev. **C4** (1971) 2185.

28. P. Möller, G. A. Leander and J. R. Nix, Z. Phys. **A323** (1986) 41.

29. J. R. Nix and A. J. Sierk, Phys. Rev. **C15** (1977) 2072.

30. S. Bjørnholm and W. J. Swiatecki, Nucl. Phys. **A391** (1982) 471.

31. P. Armbruster, Ann. Rev. Nucl. Part. Sci. **35** (1985) 135.

32. F. P. Hessberger, S. Hofmann, W. Reisdorf, K.-H. Schmidt, H. J. Schött, P. Armbruster, R. Hingmann, B. Thuma and D. Vermeulen, Z. Phys. **A321** (1985) 317.

33. J. P. Blocki, H. Feldmeier and W. J. Swiatecki, Nucl. Phys., to be published.